Satellite-based DNI nowcasting based on a sectoral atmospheric motion approach

Marion Schroedter-Homscheidt, Niels Killius, Diana Mancera Guevara, Tobias Sirch, Natalie Hanrieder, Stefan Wilbert, and Zeyad Yasser

Citation: AIP Conference Proceedings **2033**, 190015 (2018); doi: 10.1063/1.5067200
View online: https://doi.org/10.1063/1.5067200
View Table of Contents: http://aip.scitation.org/toc/apc/2033/1
Published by the American Institute of Physics

Satellite-based DNI Nowcasting Based on a Sectoral Atmospheric Motion Approach

Marion Schroedter-Homscheidt[1a], Niels Killius[1], Diana Mancera Guevara[1], Tobias Sirch[2], Natalie Hanrieder[3], Stefan Wilbert[3], and Zeyad Yasser[4]

[1]*German Aerospace Center (DLR), German Remote Sensing Data Center (DFD), Oberpfaffenhofen, Germany*
[2]*German Aerospace Center (DLR), Institute of Atmospheric Physics, Oberpfaffenhofen, Germany*
[3]*German Aerospace Center (DLR), Institute of Solar Research, Almeria, Spain*
[4]*TSK Flagsol, Cologne Germany*

[a)]Corresponding author: marion.schroedter-homscheidt@dlr.de

Abstract. Within European Commission's FP7 DNICast project a nowcasting scheme based on Meteosat Second Generation cloud imagery and cloud movement tracking was further developed. It uses a sectoral approach and answers the question at which time any cloud structure will affect the power plant. It distinguishes between thin cirrus clouds and other clouds, which typically occur in different heights in the atmosphere and move in different directions. Also, their optical properties are very different - especially for the calculation of direct normal irradiance (DNI) as required by concentrating solar power plants. The method is also applied in ESA's CSP-FoSyS project developing a nowcasting and forecasting system. This paper shortly discusses the method and provides a comparison against an optical flow method. This comparison distinguishes between various cloud types. The study also provides an example how jumpiness and percentiles are part of the nowcasting 'message' and how they can be used quantitiatively in a first approach.

THE SECTORAL ATMOSPHERIC MOTION APPROACH

This method applies a receptor-like approach tracking only clouds which are coming closer to the power plant (red color in Figure 1) and discriminating between thin cirrus and other cloud types. The algorithm [1] has undergone a major revision resulting now in the nowcasting of DNI percentiles being derived out of cloud optical depth (COD) percentiles. These cloud optical depth percentiles are obtained from the pixel to pixel variability in the upcoming cloud system.

The AVHRR Processing scheme Over cLouds Land and Ocean (APOLLO) has been adapted to the MSG SEVIRI instrument. It discretizes all pixels into four different groups called cloud-free, fully cloudy, partially cloudy (i.e. neither cloud-free nor fully cloudy) and snow/ice-contaminated, before deriving physical properties [2,3]. Within APOLLO, clouds are categorized into three layers according to their top temperature (low, medium, high). The layer boundaries are set to 700 hPa and 400 hPa. The associated temperatures are derived from standard atmospheres. Further, each fully cloudy pixel is checked to see whether it is a thick or thin cloud, depending on its 11 µm and 12 µm brightness temperatures and, during daytime, its channel 0.6 µm and 0.8 µm reflectances. Optically thin clouds (with no thick clouds underneath) are taken as ice clouds, i.e. cirrus, whereas thick clouds are treated as water clouds.

From the MSG/APOLLO-based cloud physical parameters especially the cloud mask and the cloud type discrimination into water/mixed phase and thin ice phase clouds are used in a pixel-wise resolution. Additionally, the cloud optical depth (COD) is used. The receptor model looks for the movement of a cloud towards the power plant. It performs the following steps:

SolarPACES 2017
AIP Conf. Proc. 2033, 190015-1–190015-7; https://doi.org/10.1063/1.5067200
Published by AIP Publishing. 978-0-7354-1757-1/$30.00

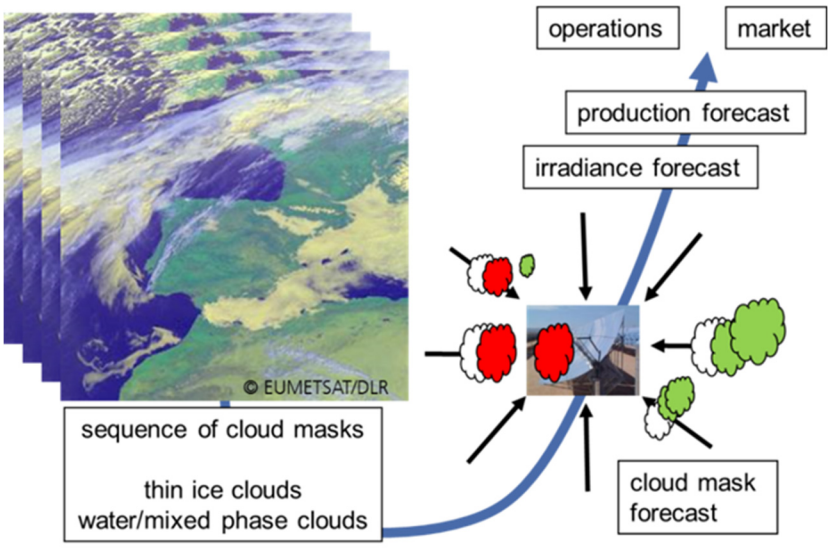

FIGURE 1. Scheme of the receptor like sectoral nowcasting

Satellite pixels in a 49 x 49 pixel neighborhood are remapped from a latitude-longitude grid (SEVIRI satellite projection) into an x-y kilometer polar coordinate system with the location of interest in the center.

The algorithm uses two separate cloud masks – one consists of thin ice phase clouds only, the other consists of all pixels being classified as water or mixed phase cloud. Typically, the thin ice clouds are cirrus-like clouds in higher altitudes. They often have different directions of movement, are larger scale features with small COD and a large variability of COD.

A low pass filtering of the cloud mask is performed. Small clouds of just a few pixels size are difficult to be tracked and most likely will disappear as individual clouds through a merging process with neighboring clouds or will increase or shrink over the nowcast horizon in an unpredictable manner. Therefore, they only enhance the noise in the signal without adding to the method's accuracy.

The nowcast is being initialized with the situation being cloudy or not cloudy at the pixel at the start of the nowcast. Clouds but also cloud gaps moving towards the power plant are tracked within each sector over 3 time slots of satellite imagery. The surroundings of the location of interest are separated into 32 sectors with equal angular distribution. All pixels having a polar angle within the sector are mapped onto the bisecting line inside the sector at the distance to the central pixel. By that a vector of cloud mask values (cloudy, cloud free) is created along each sector's bisecting line and for both cloud masks separately. The more detailed structure inside the two-dimensional sector is reduced to a one-dimensional vector by this approach. This reduces the spatial resolution, but also increases the clearness of the signal itself. Within this one-dimensional vector again a low pass filter is performed. Cloud gaps up to 7 km along each bisecting line are set to cloudy as well to avoid small gaps being created by the mapping to the bisecting line process. Clouds being only 1 pixel long are set to cloud free on the other hand.

For each bisecting line vector a search of sign changes between 0 and 1 (cloud free and cloudy) is performed. They represent the borders of cloud systems. Their movement towards and away from the central pixel is monitored. Only if a sign change is found in both images this sector is used for a cloud movement vector derivation in this sector. Sectors with only one sign change or differing sign changes are excluded as they do not contribute a clear signal of movement towards the central pixel. Also, sectors with two strongly differing vectors between image 1 and 2 and image 2 and 3 are excluded. The criterion set is three times the smallest vector length. If the second vector is longer than this, again the sector is excluded as providing no clear signal. This is frequently seen if clouds are moving far away from the central pixel with a significant component normal to the bisection line. They are unlikely to move to the central pixel, but create a strongly varying signal of the movement component along the section line. As the movement normal to the section line is not monitored explicitly, this is used as an indicator to detect such cases. For each valid sector a movement vector is calculated along the bisection line and for each sign change. According to the vector length, the time of reaching the central pixel is marked in the nowcasting vector describing the cloud mask situation at the central pixel as evolution over time. Four cases are therefore tracked separately:

Arrival of a thin cirrus type cloud and end of such a cloud period, as well as arrival of a thick water/mixed phase cloud and the end of such a cloud period. By that a vector of upcoming thin and thick cloud situations over time is created.

Finally, each nowcast is provided for percentiles of DNI – being generated out of the spatial variability of the DNI in the sector from where the actual cloud is reaching the power plant site. Minimum and maximum values are given together with P10, P50, and P90 values. Within this study, only the P50 values are used and the provided variability information is neglected. Please note the temporal smoothness of each percentile as this method transfers the spatial variability as seen by the satellite into a percentile information.

COMPARISON AGAINST AN OPTICAL FLOW METHOD

In parallel, the DNICast project also worked on a cloud motion vector approach using optical flow methods [4]. Both approaches are compared.

In this paper, both approaches are compared. Both methods show a similar small mean bias error over the whole nowcast horizon. The mean absolute error (MAE) is similar until 40 minutes and afterwards the optical flow performs better with respect to the MAE. With respect to the root mean square error (RMSE, see Fig. 2), the sectoral receptor model performs better until 40 minutes and afterwards the RMSE slightly larger compared to the optical flow method. Similar RMSE are reached for both approaches from 220 minutes forecast lead time onwards.

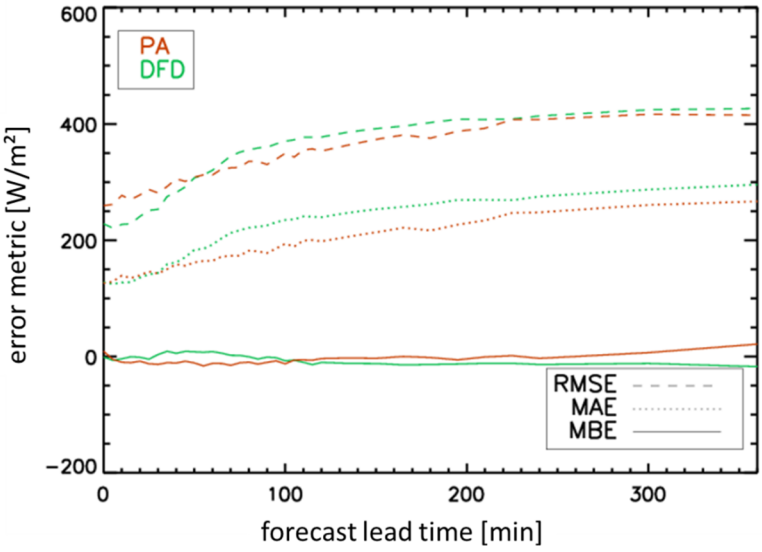

FIGURE 2. Overall comparison results of an optical flow (red) and the sectoral receptor approach (green) versus 1 min pyrheliometer observations from March to May 2013 at DLR-PSA.

This study especially looked into the verification of both nowcast schemes with respect to various cloud conditions. Scattered, broken/overcast, cirrus, and clear situations are separated in the verification as previously used in [5] are evaluated. This class-wise verification provides insight when either the optical flow and/or the P50 percentile as derived from the sectoral approach perform better or where they perform quite similar (Fig. 3). Overall, we have 4325 cases, 1936 being classified as clear, 509 as optically thin, 966 as broken/overcast and 914 as scattered cases.

Below 70 minutes forecast horizon the receptor method shows smaller RMSE for clear sky, scattered and thin ice clouds and it also has slightly lower RMSE values for broken/overcast conditions in the first 30 minutes. After that the optical flow method performs better. The biases of the receptor method show a very strong increase between 60 and 100 minutes in thin ice, broken/overcast and clear conditions. Only in the scattered cloud cases this is not found. Both in broken/overcast and optically thin cloud conditions, all methods show an increase of MBE with forecast lead time, but the DFD method shows the largest increase of MBE with forecast lead time. This is an indication that all, but especially the DFD method, tend to predict the situation as being clear while it is cloudy. DFD developers

have observed that in some cases the pixel window in the nowcasting scheme selected is too small. This increase is being under further investigation currently.

Having found a close to zero MBE for the DFD method is supporting that overall, the cloud optical properties used in the radiative transfer in the DFD method are well met for optically thick clouds. Only in the cases of broken/overcast clouds, this cannot be discriminated from the error of providing a too clear nowcast. But in the case of scattered clouds, this effect disappears and overall no bias remains, which would indicate an issue in the cloud optical properties of optically thick clouds. This possibility to discriminate between both possible sources of nowcast error is an important finding when using the cloud area type classification as additional analytics.

On the other hand, for optically thin clouds, we find a positive MBE for all methods around 30 to 50 W/m². This supports the assumption that, generally, the COD of optically thin clouds is slightly underestimated and that the DNI is overestimated. Having in mind that the DNI is very sensitive to small changes in COD in the very small COD range of optically thin clouds, it is assumed that the overall COD underestimation is rather small. Nevertheless, due to the high sensitivity of DNI to the small COD value range, it shows up as a non-negligible MBE.

RMSE values for scattered cloud situations are remarkably higher than in all other classes. This is expected due to the higher natural variability of DNI in such cases. Especially in scattered cloud situations, cloud speed and direction of cloud movement leads to large uncertainties. Clouds just need to move some degrees in a different direction and a cloudy sky nowcast will be made instead of a clear sky nowcast. If speed is not correct, the arrival of the cloud is forecasted at the wrong time and the departure as well. Additionally, scattered cloud fields may consist of cumulus clouds being created within 10s of minutes and disappearing afterwards while the air flows without 'transporting' the cloud furtheron. Both effects result in twice as large errors within short time.

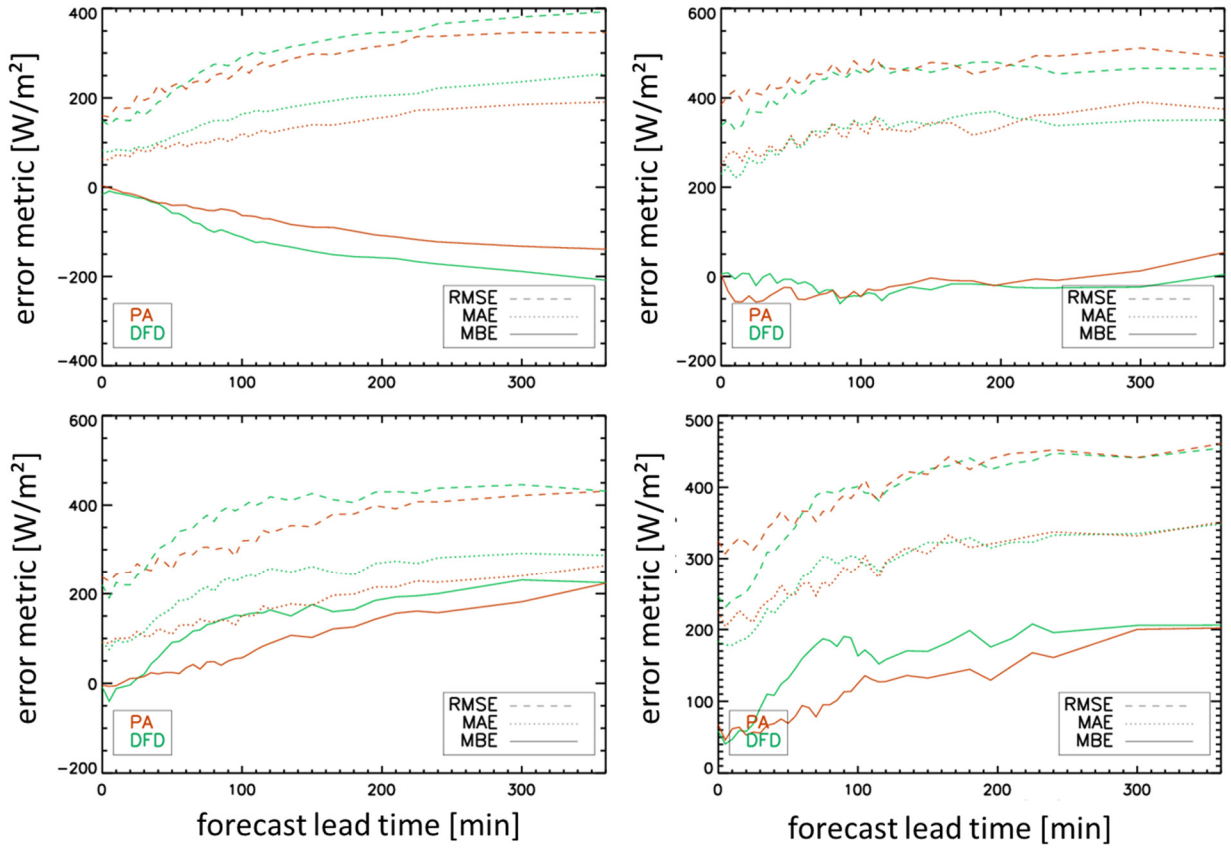

FIGURE 3. Error metrics for 4 cloud area types: a) clear sky, b) scattered, c) broken overcast, d) thin ice clouds

THE INFORMATION CONTENT OF A PERCENTILE RANGE FORECAST AND THE JUMPINESS FROM NOWCAST TO NOWCAST

Both the jumpiness from each nowcast to the next nowcast and the percentile range in each individual nowcast turn out to be a promising indicator of the real 1 min variability that needs to be expected in the actual situation. The actual 1 min values and their real variability in cloud conditions are out of reach of the satellite-based nowcasting, but using the percentiles and monitoring the jumpiness of the nowcasts provide a good indicator of the expected 1 min DNI variability.

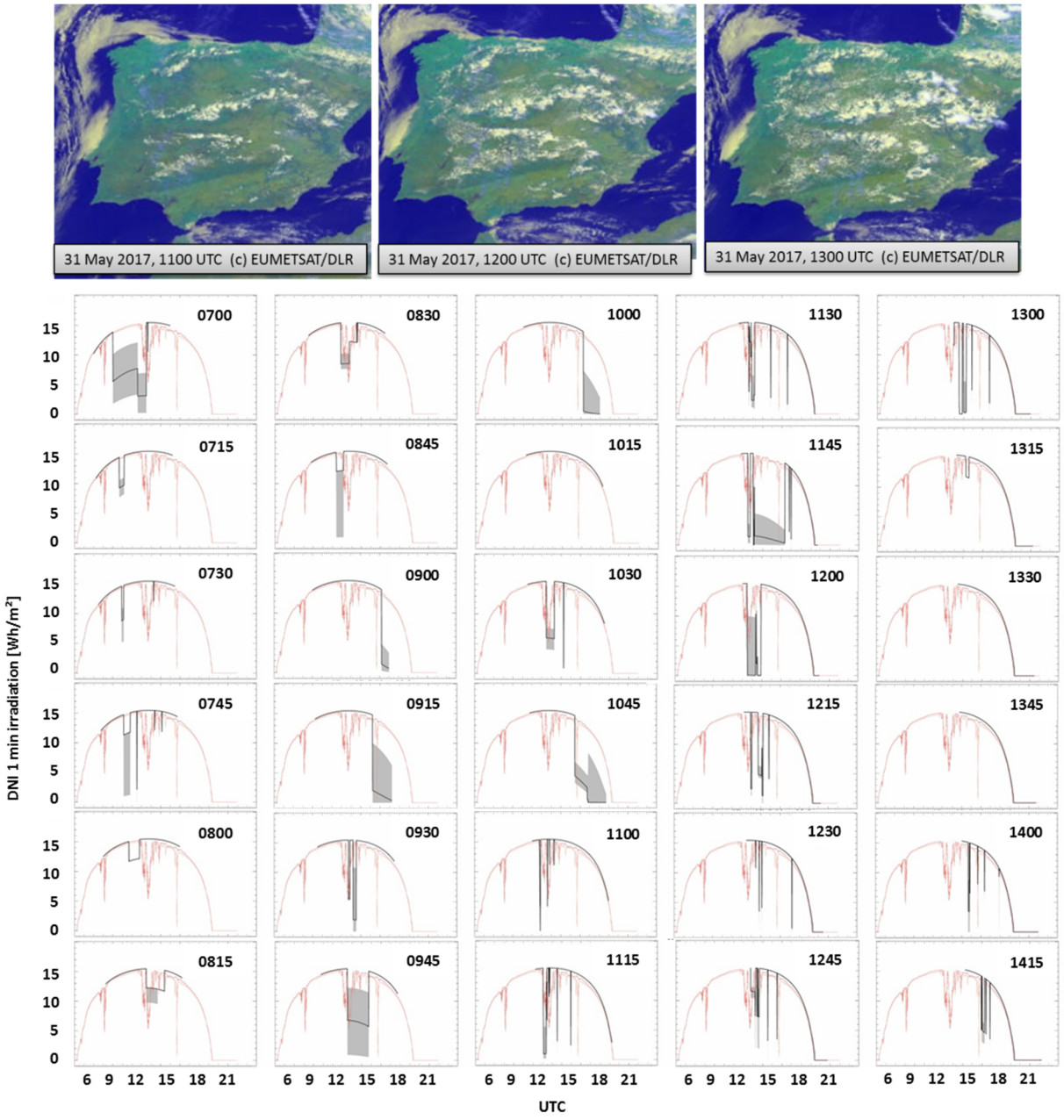

FIGURE 4. Example of cloud fields and DNI nowcasts on the 31st May 2017 – illustrating variable DNI conditions by both a temporal jumpiness from nowcast to nowcast and by the spatial variability as given in the percentile range. The nowcasts start from 0700 (upper left) and are given up to 1415 UTC (lower right). They are ordered first vertically from top to bottom, and then from left to the right as temporally consecutive order.

In this paper we discuss a single day to illustrate the concept. The 31st May 2017 was dominated by a large number of cumulus cloud fields over elevated areas in Spain. Cumulus clouds were created and disappeared – partly within a 30 minute time frame. The three satellite images from 11, 12 and 13 UTC give an overview, but this static graphical presentation is by far not sufficient to demonstrate the fast evolution and disappearance of the individual cumulus clouds. For the nowcast scheme such a quickly changing situation is a major challenge as movements are anticipated which do not exist – and if the nowcasting is good, it will at least show the change by changing the nowcast in the same speed. Unfortunately, for the user this may be confusing as the nowcast is changing rapidly. But on that day that was correct. Therefore, quick changes in nowcasting can be seen as some information to be noticed and taken into account and should not be seen as a deficiency.

Besides these rapidly changing cumulus cloud fields a cirrus field is crossing Spain, being in parallel to the Portuguese – Spanish border at 1100 and crossing around 12:30 UTC the LaAfricana site. It is visible as a darker blue, a bit fuzzy cloud pattern in the satellite imagery also by the eye. This actually causes a drop-down to DNI values between 400 and 600 W/m² with a fast changing pattern between 12 and 13:30 UTC. The challenge for the nowcasting is to meet this cirrus cloud, while the cumulus clouds around are coming and disappearing but not coming to the power plant site.

Fig. 4 provides all nowcasts from 0700 to 1415 UTC of that day. The 0700 forecast is given on the upper left, followed by the 0715 nowcast just below. So, the time axis is running first from top to bottom, than again from top to bottom in the 2nd column and further on from the left to the right column. The 1415 UTC nowcast is the lower right edge.

Looking into the 0700 UTC nowcast, a long period with medium DNI is nowcasted, but this already has some large uncertainty – being visible in the large P10/P90 percentile ranges. The next nowcast is changed dramatically, it predicts a short period of low DNI, but this is further reduced in the next nowcast at 0730. At 0800, another indication of a low value period is given, but again with a large percentile range. Around 0830 and 0845 an event around noon is nowcasted, but it disappears in the next two nowcasts. Afterwards at 0930, it is nowcasted again, while at 1000 it is not nowcasted anymore, but at 1030 it is seen again. Later, when coming in the very short term nowcasting range at 1100 onwards, the pattern remains not continuously and is very similar to the reality. But again, the situation after the noon event is nowcasted differently in each consecutive nowcast. It can be seen how both the jumpiness from nowcast to nowcast and the percentile range as given from the spatial cloud variability give indications of a difficult to predict, quickly varying situation. We recommend making use of this jumpiness and percentile ranges when assessing the upcoming DNI quality and variability. The individual 1 min value is out of reach in satellite-based nowcasting, but this variability is of additional use compared to the individual nowcast.

USE OF PERCENTILE RANGES AS UNCERTAINTY ESTIMATE IN A NOWCAST MERGING PROCEDURE

Finally, the relevance of nowcasted DNI percentiles is discussed. These percentiles are of high interest for the dispatch optimization, the plant operation and the combination of the nowcasts with other nowcasting methods. In [6] the DNI percentiles as well as the minimum and maximum values of nowcasted DNI are used to derive the absolute uncertainty of the nowcast for cloudy situations. The absolute uncertainty has to be estimated to include the sectoral atmospheric motion approach within an uncertainty-weighted nowcast combination.

To estimate the absolute uncertainty Δ, two different options have been tested:

1. $\Delta_{min,max} = \frac{DNI_{min} - DNI_{max}}{2}$
2. $\Delta_{percentiles} = \frac{DNI_{p90} - DNI_{p10}}{2.5631}$

To estimate the absolute uncertainty with the P10 and P90 percentiles, the standard deviation can be calculated assuming that the DNI nowcast can be represented with a normal distribution which has been done in option 2. These options can only be applied for possibly cloudy situations, otherwise the absolute uncertainty is estimated to be zero as DNI_{p90}, DNI_{p10} as well as the minimum and maximum values are equal. In the investigated time period of [4] (12 selected months between 2010 and 2015 for PSA, 1 minute temporal resolution of the nowcast, 15 minutes refresh rate) clear-sky situations have been nowcasted in about 46% of all examined time steps. For these situations, a fixed absolute uncertainty of 200 W/m² has been chosen for the combination with other nowcasting products. In

about 28% no nowcasted DNI as well as minimum, maximum and percentiles are available due to low solar elevation angles.

For the remaining time steps, the absolute deviations Δmin,max and Δpercentiles are plotted in Fig. 5. It can be seen that in all situations, Δmin,max delivers larger estimated absolute uncertainties than Δpercentiles. It has to be noted that assuming a normal distribution of the nowcast is a strong assumption and especially for cases with small or thin clouds passing through the pixel this assumption might not be valid.

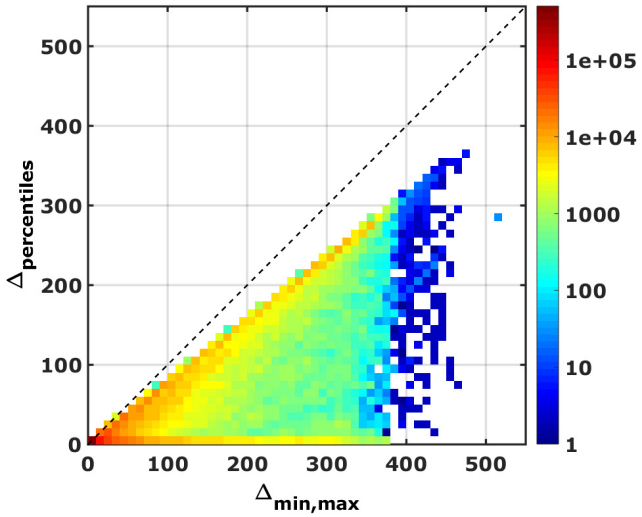

FIGURE 5. Inter-comparison of the derived absolute uncertainties $\Delta_{min,max}$ and $\Delta_{percentiles}$ with the options 1 and 2 for 12 months nowcasts for PSA. Zeros have been excluded. The color distribution displays the number of data points per grid point (logarithmic color scale).

In future work, the percentiles can be used to fit certain normal distributions for each time step and derive the standard deviation from these distributions to estimate the absolute uncertainty for possibly cloudy situations.

ACKNOWLEDGMENTS

The DNICast project (http://www.dnicast-project.net/) has received funding from the European Union's Seventh Programme for research, technological development and demonstration under grant agreement No 608623. The practical application of this research is tested e.g. in the CSP-FOSyS project (https://business.esa.int/projects/csp-fosys), which is an ESA co-funded ESA Artes Applications project.

REFERENCES

1. M. Schroedter-Homscheidt and G. Gesell, Verification of Sectoral Cloud Motion Based Direct Normal Irradiance Nowcasting from Satellite Imagery. SolarPaces 2015, 13-16 Oct 2015, Capetown, South Africa.
2. Kriebel, K. T., Saunders R. W., and Gesell, G.: Optical properties of clouds derived from fully cloudy AVHRR pixels. Beitr. Phys. Atmosph., 3, 62, 165-171, 1989
3. Kriebel, K. T., Gesell, G., Kästner, M., and Mannstein, H.: The cloud analysis tool APOLLO: Improvements and validations, Int. J. Remote Sensing, 12, 24, 2389-2408, doi: 10.1080/01431160210163065, 2003
4. T. Sirch, L. Bugliaro, T. Zinner, M. Möhrlein, M. Vazquez-Navarro, Cloud and DNI nowcasting with MSG/SEVIRI for the optimized operation of concentrating solar power plants, Atmos. Meas. Tech., 10, 409-429, 2017.
5. M. Schroedter-Homscheidt, A. Benedetti, N. Killius, Verification of ECMWF and ECMWF/MACC's global and direct irradiance forecasts with respect to solar electricity production forecasts, Meteorologische Zeitschrift, 26, 1, 1-19, 2017.
6. L. Ramirez et al., Optimized DNI forecast using combinations of nowcasting methods from the DNICast project. Abstract submitted to the SolarPACES conference 2017.